

---

# MULTI-CLASS AND MULTI-TASK STRATEGIES FOR NEURAL DIRECTED LINK PREDICTION

---

Claudio Moroni <sup>1,2</sup>, Claudio Borile<sup>2</sup>, Carolina Mattsson<sup>2</sup>, Michele Starnini<sup>2,3</sup>, and André Panisson<sup>2</sup>

<sup>1</sup>Dedagroup, Torino, Italy

<sup>2</sup>CENTAI Institute, Torino, Italy

<sup>3</sup>Department of Engineering, Universitat Pompeu Fabra, Barcelona, 08018, Spain

## ABSTRACT

Link Prediction is a foundational task in Graph Representation Learning, supporting applications like link recommendation, knowledge graph completion and graph generation. Graph Neural Networks have shown the most promising results in this domain and are currently the de facto standard approach to learning from graph data. However, a key distinction exists between Undirected and Directed Link Prediction: the former just predicts the existence of an edge, while the latter must also account for edge directionality and bidirectionality. This translates to Directed Link Prediction (DLP) having three sub-tasks, each defined by how training, validation and test sets are structured. Most research on DLP overlooks this trichotomy, focusing solely on the "existence" sub-task, where training and test sets are random, uncorrelated samples of positive and negative directed edges. Even in the works that recognize the aforementioned trichotomy, models fail to perform well across all three sub-tasks.

In this study, we experimentally demonstrate that training Neural DLP (NDLP) models only on the existence sub-task, using methods adapted from Neural Undirected Link Prediction, results in parameter configurations that fail to capture directionality and bidirectionality, even after rebalancing edge classes. To address this, we propose three strategies that handle the three tasks simultaneously. Our first strategy, the Multi-Class Framework for Neural Directed Link Prediction (MC-NDLP) maps NDLP to a Multi-Class training objective. The second and third approaches adopt a Multi-Task perspective, either with a Multi-Objective (MO-DLP) or a Scalarized (S-DLP) strategy. Our results show that these methods outperform traditional approaches across multiple datasets and models, achieving equivalent or superior performance in addressing the three DLP sub-tasks.

## 1 Introduction

Graphs are a natural way to represent complex systems. Examples include social networks, financial transaction networks, power grids, and neuronal connectivity [1, 2]. These systems can be modeled using different types of graphs, ranging from simple networks to more sophisticated structures like Knowledge Graphs [3], Dynamic Graphs [4], or Bipartite Graphs for recommender systems [5]. Given the broad applicability of graphs, Representation Learning on graph-like data structures has become essential, with core tasks including node classification, link prediction and graph classification.

In this work, we focus on Link Prediction [6], particularly its Directed variant. Recently, Graph Neural Networks (GNN)-based models, such as Graph Autoencoders, have been devised to address Link Prediction tasks [7–19], establishing the field of Neural Link Prediction. These models have several important applications, including completing knowledge graphs [20], serving as baseline for deep graph generation [7, 21] and pre-processing transaction networks [22]. The recent literature primarily focuses on undirected applications [23–25], with few studies mentioning directed cases [26]. Direction can be core to the application itself, in some domains. With citation graphs, for instance, citing and being cited have substantively different meanings. Moreover, incorporating edge direction has been shown to improve learning for node classification across different types of graphs [27]. Even so, the complexity of Directed Link Prediction (DLP) is often overlooked and it has been argued that this limits progress in NDLP [17].

Neural Directed Link Prediction (NDLP) requires a model that is capable of representing edge direction and a training strategy that effectively learns directionality. Not all GNNs can represent edge direction. Graph Autoencoders, for example, often use decoder implementations where probabilities for edges  $(u, v)$  and  $(v, u)$  are the same by design [17]. We refer to these models as NDLP-incapable. But even NDLP-capable models can fail to learn edge directionality when the training strategy is borrowed from Neural Undirected Link Prediction (NULP). Typically, NULP models are trained and evaluated on random subsets of positive and negative undirected edges [7–12, 19]. Now, on a sparse directed graph, it is statistically unlikely that a random subset of negative directed edges would include the reverse of a randomly sampled positive directed edge. This allows models to ignore edge direction without incurring a penalty. Indeed, using the NULP approach to training and evaluating NDLP models [13–16] can lead to NDLP-incapable models performing deceptively well.

Training and evaluation for NDLP is more complex. Three sub-tasks have been devised in the recent literature to comprehensively evaluate distinct aspects of DLP [17–19, 28]. The ‘‘General’’ DLP task is the classic adaptation of the approach used in ULP to the directed case. This is then complemented with two other binary classification sub-tasks designed to test a model’s ability to distinguish edge directions. Namely, the ‘‘Directional’’ and ‘‘Bidirectional’’ sub-tasks. Prior work has shown that NDLP-capable models can learn to perform well on each of the three sub-tasks [17–19, 28] and that there is a trade-off among them [18]. However, prior approaches do not consider training strategies that can handle these three sub-tasks simultaneously.

Here we propose three learning strategies to improve performance across DLP sub-tasks, simultaneously. The first strategy, *Multi-Class Directed Link Prediction* (MC-DLP), maps DLP to a four-class classification task. This framework distinguishes between unidirectional positives, unidirectional negatives, bidirectional positives, and bidirectional negatives, ensuring balanced contributions to the training loss. The other two approaches recognize the Multi-Task nature of DLP, simultaneously training on simultaneously constructed *General DLP*, *Directional* and *Bidirectional* training sets. Drawing from the literature on Multi-Objective [29] and Scalarization [30] methods, we propose *Multi-Objective Directed Link Prediction* (MO-DLP) and *Scalarization-based Directed Link Prediction* (S-DLP) strategies to handle these tasks more effectively. Each of our three training strategies incentivize NDLP-capable models to perform well across different aspects of DLP, and our results show that better training strategies can be just as important as better models in advancing the state of Neural Directed Link Prediction.

The remainder of this paper is organized as follows: Section 2 covers the background concepts and related work, highlighting their relevance to our approach. In Section 3, we detail the proposed multi-class and multi-task strategies. Section 4 outlines the experimental setup, describes the datasets and presents a performance comparison of various models across all strategies and datasets. Finally, Section 5 provides concluding remarks.

## 2 Background and Related Work

In this section, we introduce the notation and review key concepts and prior research relevant to Neural Directed Link Prediction (NDLP). We briefly discuss foundational work in Graph Neural Networks and their applications in undirected link prediction, then go on to examine approaches for incorporating directionality. This serves to highlight certain limitations and the need for more comprehensive training strategies.

### 2.1 Notation

Given a directed graph  $G = (V, E)$  with  $N = |V|$  nodes where  $E \subseteq V \times V$ , and given  $u, v \in V$  we say that:

- $(u, v)$  is *negative bidirectional*  $\iff (u, v) \notin E \wedge (v, u) \notin E$ ;
- $(u, v)$  is *negative unidirectional*  $\iff (u, v) \notin E \wedge (v, u) \in E$ ;
- $(u, v)$  is *positive unidirectional*  $\iff (u, v) \in E \wedge (v, u) \notin E$ ;
- $(u, v)$  is *positive bidirectional*  $\iff (u, v) \in E \wedge (v, u) \in E$ ;

Moreover, we denote  $A \in \{0, 1\}^{N \times N}$  as  $G$ ’s adjacency matrix, and  $X \in \mathbb{R}^{N \times F}$  as node features.

### 2.2 Graph Neural Networks

Graph Neural Networks (GNNs) are currently the de facto standard approach for directed link prediction. Message Passing Neural Networks (MPNNs) [31–34] is the most general framework for GNNs, and other frameworks such as Spectral Graph Convolutional Neural Networks (SGCNNs) [35, 36] can be mapped to the MPNN framework.

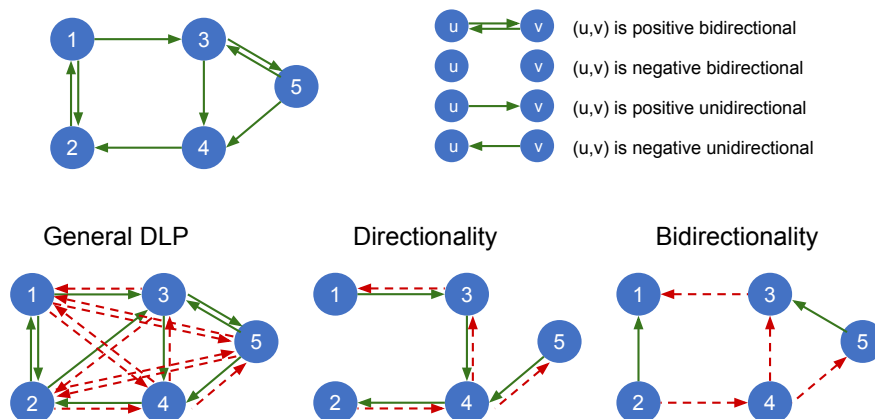


Figure 1: From a graph  $G$  (top panel), for each task definition, green edges are the positive class and red edges are the negative class. In *General DLP*, any absent directed edge can be selected as negative. For *Directionality* prediction, unidirectional edges are positive, with their inverses as negatives. For *Bidirectionality* prediction, one direction of bidirectional edges is positive, and the reverse of unidirectional edges is negative.

Applications concern pharmaceutical industry, material science [37], time series [38], anti-money laundering [39–42]. In the remainder of this section, we describe the general MPNN paradigm, current state-of-the-art deep learning technique for Graph Representation Learning.

MPNNs elaborate successive hidden representations for each node  $v$  aggregating messages from its neighbors.

Given  $z_v^{(k)}$  as the  $k$ -th layer embedding of node  $v$  (with  $z_v^{(0)}$  equalling  $v$ 's feature vector  $x_v$ ), GNNs compute the next layer embedding  $z_v^{(k+1)}$  through the following relation:

$$z_v^{(k+1)} = f^{(k)} \left( m_s^k(z_v^{(k)}), A^{(k)} \left( \left\{ m_n^k(z_u^{(k)}) \mid u \in N(v) \right\} \right) \right) \quad (1)$$

Where  $f^{(k)}$ ,  $A^{(k)}$ ,  $m_s^k$  and  $m_n^k$  are, respectively, the layer-specific update function, the aggregation function, the self-information and message functions.  $N(v)$  indicates the neighborhood of node  $v$ .

If we consider  $K$  layers in total, the last embedding of each node  $z_v \equiv z_v^{(K)}$  can be used for downstream tasks such as node classification, link prediction, and graph classification. For link prediction, a *decoder* function takes as input the representation of two nodes,  $z_u, z_v$  and outputs a normalized score representing the probability of an edge  $(u, v)$  being present. For the undirected case, the decoder function can be the scalar product followed by a sigmoid function,  $DEC(z_u, z_v) = \sigma(z_u \cdot z_v)$ , or a neural network such as a MLP. The scalar product, being symmetric in  $u$  and  $v$ , is an example of a decoder unable to learn directionality.

### 2.3 Neural Directed Link Prediction

This work considers three sub-tasks for directed link prediction, as presented in [17]. Figure 1 shows a representation of the positive and negative classes that define the *General Directed Link Prediction (General DLP)*, *Biased Directional Negative Samples Link Prediction (Directional)*, and *Bidirectionality Prediction (Bidirectional)* tasks. These classes are the basis for selecting the (directed) edges used in the testing and evaluation of NDLP-capable models on DLP in the most relevant recent literature.

We focus on NDLP-capable models that use Graph Autoencoder techniques. [13] develops an extension of the Weisfeiler-Lehman kernel [43] which is then used as a basis to define a source/target-like [17] graph autoencoder for directed graphs; however, the model is only tested on the *General DLP* sub-task. [18] defines a GCN for directed graphs where the aggregation is performed by a complex, hermitian laplacian. This model is tested across all three tasks, although for each of them, a different parameter set is inferred. To the best of our knowledge, [17] devises the earliest GNN-based autoencoders for NDLP, and is among the first to highlight the intrinsic differences between NDLP and NULP; Their work is also responsible for one of the earliest usage of the *General DLP*, *Directional* and *Bidirectional* sub-tasks in a neural setting. Similarly to [18], the authors of [17] do not find one parameter set for all three tasks for each model. [19] endows cluster information in node embeddings, but, similarly to [17], trains and tests over the *Directional* and *Bidirectional* tasks using two different training graphs. [28] produces unsupervised source/target node embeddings by adversarially training a neural pair of generator and discriminator on the graph topology; the

final model performs simultaneously well on the *General DLP* and *Directional* task, but it is not evaluated on the *Bidirectional* task.

Although we will experiment with different models, it is not our aim to sponsor anyone in particular. Rather, we propose learning strategies that can be used with *any* NDLP-capable model to encourage encoding directionality and strike a better balance among the performances on sub-tasks of NDLP. Therefore our work is much more in the spirit of [44], a representation learning framework that argues in favor of masking compared to full-graph training. Unfortunately, [44] has been developed and tested on undirected graphs only, so its extension to directed graphs could be a future research avenue.

### 3 Strategies for Neural Directed Link Prediction

In the previous section, we discussed that NDLP has recently been described as three distinct sub-tasks: General DLP, Directional, and Bidirectional. Simultaneously addressing these requires more than adapting the classic approach to (undirected) link prediction. In this section, we formalize two training strategies that are in principle applicable to every NDLP-capable encoder-based MPNN and encourage such models to learn to encode directionality.

#### 3.1 Multi-Class Strategies for Neural Directed Link Prediction

As anticipated in Section 1, we assume that the reason why prior works are generally not able to infer a single model that performs well on all three sub-tasks is related to an unaddressed imbalance between unidirectional and bidirectional edges’ contributions to the training loss. We note that this imbalance should be dealt with without compromising the positive/negative edges’ reweighting. Therefore we propose to simultaneously balance positives vs negatives and unidirectional vs bidirectional edges using the following Multi-Class Neural Directed Link Prediction (*MC-NDLP*) strategy.

Given a GNN model that computes  $d_K$ -dimensional embeddings  $z_v, \forall v \in V$ , we may compute logits for each of the four classes listed in Section 2.1 by applying an MLP to the concatenation of the embeddings. The MLP must take  $2d_K$  input dimensions and output 4 logits, and can be arbitrarily deep:

$$[\hat{l}_{uv}^{nb}, \hat{l}_{uv}^{nu}, \hat{l}_{uv}^{pu}, \hat{l}_{uv}^{pb}] = \text{MLP}(z_u || z_v), \quad (2)$$

where  $\hat{l}_{uv}^m, m \in \{nb, nu, pu, pb\}$  denote the model’s output logits for the edge  $(u, v)$  being negative bidirectional, negative unidirectional, positive unidirectional, or positive bidirectional as defined in §2.1.

Notably, *MC-NDLP* is also compatible with any graph autoencoder that makes use of specific decoders which output only one logit  $\hat{l}_{uv}$ , that is, the model output for the presence of a directed edge  $(u, v)$  [13, 17]. We can turn the standard binary classification task for NDLP into a 4-class classification task by transforming the output logit into a probability via e.g., a sigmoid

$$\hat{p}_{uv} = \sigma(\hat{l}_{uv}) \quad (3)$$

and defining:

$$[\hat{p}_{uv}^{nb}, \hat{p}_{uv}^{nu}, \hat{p}_{uv}^{pu}, \hat{p}_{uv}^{pb}] = [(1 - \hat{p}_{uv})(1 - \hat{p}_{vu}), \\ (1 - \hat{p}_{uv})\hat{p}_{vu}, \\ \hat{p}_{uv}(1 - \hat{p}_{vu}), \\ \hat{p}_{uv}\hat{p}_{vu}]. \quad (4)$$

We note that Eq. 4 assumes statistical independence between  $\hat{p}_{uv}$  and  $\hat{p}_{vu}$ , which are both conditioned on  $A$  and  $X$ . In fact, most autoencoders model  $\hat{p}_{uv} = \hat{P}(e_{uv} | A, X)$  where  $e_{uv} = 1 \iff (u, v) \in E$  otherwise it equals 0 [7], and Eq. 4 naturally extends these univariate autoencoders. Please refer to Appendix A.3 for more details.

We can then define a weighted Multi-Class cross-entropy loss function:

$$\mathcal{L}_{MC-NDLP}(\Theta) = - \sum_{c \in \mathcal{C}} \sum_{uv \in \mathcal{T}} w_{y_{uv}} \mathbb{I}(y_{uv} = c) \log(\hat{p}_{uv}^{y_{uv}}), \quad (5)$$

where  $C = \{nb, nu, pu, pb\}$ ,  $T$  is the *General DLP* training set (see §3.3),  $\mathbb{I}$  is the indicator function and  $y_{uv} \in C$  is the ground-truth class of the edge  $(u, v)$ , and  $\hat{p}_{uv}^{y_{uv}}$  is the model’s output probability of edge  $(u, v)$  belonging to the ground-truth class  $y_{uv}$ . The class weight is defined as

$$w_{y_{uv}} = \frac{n_x}{n_{y_{uv}}}, \quad (6)$$

where  $n_x$  represents the number of samples in class  $x$ , where  $x$  is the most numerous class (usually  $nb$ ), and  $n_{y_{uv}}$  is the number of samples in class  $y_{uv}$ . As discussed in §1, this class reweighting mitigates the statistical imbalance between all four classes defined in §2.1.

### 3.2 Multi-Task Strategies for Neural Directed Link Prediction

Multi-Task Learning (MTL) refers to scenarios where more than one objective function must be simultaneously optimized. It is more challenging compared to single-task learning, due to the various objectives having no a priori relative importance and generally competing against each other. To simultaneously exploit the *General DLP*, *Directional* and *Bidirectional* training sources of information, we devise a multi-task objective over the three sub-tasks, defined by the binary cross-entropy loss functions on *General DLP*  $\mathcal{L}_G$ , *Directional*  $\mathcal{L}_D$  and *Bidirectional*  $\mathcal{L}_B$ .

Multi-Task learning is usually carried out in two ways:

- *Scalarization*: it prescribes to sum and weight the losses to reduce the optimization to the single-objective case:

$$\mathcal{L} = \alpha_G \mathcal{L}_G + \alpha_D \mathcal{L}_D + \alpha_B \mathcal{L}_B$$

The coefficients  $\alpha_i$ ,  $i = G, D, B$ , can be either learned or heuristically set. Despite its simplicity, heuristic implementations of Scalarization have been proven to achieve competitive performance in real use cases [30]. In this work, we set them to the validation losses (normalized between 0 and 1) of the previous epoch, to favor generalization. We name this approach *S-NDLP*;

- *Multi-Objective*: it consists in finding a parameter update rule that ensures that all losses are diminished (or left unchanged) at each optimization step. Given a model  $f_\Theta$  and the objectives  $\{\mathcal{L}_i(\Theta)\}_{i=1}^L$  to be simultaneously optimized, we say that  $\Theta_1$  *dominates*  $\Theta_2 \iff \mathcal{L}_i(\Theta_1) \leq \mathcal{L}_i(\Theta_2) \quad \forall i \in 1, \dots, L$ . Therefore, a solution  $\Theta^*$  is *Pareto-optimal* if it is not dominated by any other solution. The set of non-dominated solutions is called the Pareto set  $\mathcal{P}$ . While many Gradient-based Multi-Objective optimization algorithms with guaranteed convergence on the Pareto set have been developed, we focus for simplicity on one of the first, MGDA [29]. This algorithm is based on the observation that given the gradients associated with the individual losses, the opposite of their shortest convex linear combination points in the direction where all losses either remain constant or diminish. We name this approach *MO-NDLP*.

### 3.3 Simultaneous Splits

Train, test, and validation sets are constructed from the positive and negative classes associated to each of the three DLP sub-tasks (see Fig. 1). In [17], edges are randomly sampled from the positive classes to construct the validation and test sets separately for each sub-task. Since models are separately trained on each sub-task, the training sets can be defined as what remains when the positive samples for that sub-task are reserved. In our case, the models must be trained over the graph that remains when *all* the reserved edges are removed. In order to preserve as many edges as possible for training, sampling is done together. Specifically, for each dataset, a random 10% and 5% of all unidirectional edges are reserved for testing and validation, respectively. Moreover, a random 30% and 15% of (one direction of) all bidirectional edges are reserved for testing and validation, respectively.

Validation and test sets for the three sub-tasks are constructed using the reserved edges. All the sampled edges (unidirectional and bidirectional) are used as positives for the *General DLP* task, complemented with an equal number of randomly sampled absent directed edges as negatives. The sampled unidirectional edges are used as positives for the *Directional* task, complemented with their reverses as negatives. The randomly sampled bidirectional edges are used for the *Bidirectional* task, complemented with an equal number of the reverses of unidirectional edges randomly sampled from the remaining graph as negatives. To perform well on this task, the model must distinguish between edges whose reciprocal exists from those whose reciprocal does not.

Multi-class learning requires a single training set. As in the *General DLP* task of [17], and in the classic formulation of directed link prediction, the training set is constructed out of all remaining directed edges and all the absent edges in the incomplete training graph. In our case, these edges are sorted into the four classes defined in §2.1 for multi-class classification as described in §3.1.

Multi-task learning requires training sets for each sub-task. Here, we take the opportunity to construct our own versions of the *training* sets for the *Directional* and *Bidirectional* tasks. This is done so that the training set has similar edge statistics compared to their respective validation and test sets. In particular: for the *Directional* task, the training set is composed of all the remaining unidirectional edges (as positives) and their reverses (as negatives). This is similar to the training set for the *General DLP* task, but with the bidirectional edges removed. Finally, for the *Bidirectional* task, one direction of all the remaining bidirectional edges are used, as positives, together with an equal amount of the reverses of unidirectional edges randomly sampled from the remaining graph, as negatives.

These modifications to the sampling described in [17] make simultaneous training possible while ensuring no overlap between train and test data. Validation and test sets for the three sub-tasks are constructed using the reserved edges, and training sets are constructed using the remaining edges.

## 4 Experiments

In this section, we evaluate the effectiveness of our proposed strategies through comparative experiments using well-known datasets and DLP models. We aim to demonstrate the performance improvements of our approaches across multiple tasks and models, highlighting their ability to handle the challenges of edge directionality and directionality. All code and results are publicly available at [https://github.com/ClaudMor/Multi\\_Task\\_Multi\\_Class\\_Neural\\_Directed\\_Link\\_Prediction](https://github.com/ClaudMor/Multi_Task_Multi_Class_Neural_Directed_Link_Prediction).

### 4.1 Datasets

Our experiments are conducted on three publicly available datasets, each of which is a directed graph. As in [17], we consider two small citation networks (Cora and CiteSeer) and a larger hyperlink network (Google).

Table 1: Network statistics of the datasets used, computed using `networkx` [45].

Dataset	Nodes $ V $	Edges $ E $	Edges (undirected)	Reciprocity	Density $ E / V ^2$	Clustering
Cora	2,708	5,429	5,278	0.056	0.000741	0.131
CiteSeer	3,327	4,732	4,676	0.024	0.000428	0.074
Google	15,763	171,206	149,456	0.254	0.000689	0.343

Table 1 gives the key network statistics. The Cora and CiteSeer graphs have few bidirectional edges. For the Google graph, however, a randomly sampled directed edge will be part of a bidirectional edge around 25% of the time

. Despite the difference in size, the graph density is similar across the datasets. The local density is higher for the Google dataset, as measured by the average (directed) clustering coefficient. Edge weights and/or node attributes are not considered. In all experiments, we use one-hot encoding of the node IDs as node features [17], except for the *MAGNET* model for which we used in- and out-degree as prescribed by the authors [18]. While employing node IDs means the models are transductive, all the strategies can be extended to inductive settings by using other node features as appropriate.

### 4.2 Models

We evaluate our proposed training strategies using several NDLP-capable models from the literature, all of which follow the Graph Autoencoder paradigm. These include the Gravity-Inspired Graph Autoencoder (Gr-GAE) [17], Source/Target Graph Autoencoder (ST-GAE) [17], the DiGAE Directed Graph Auto-Encoder from [13], *MAGNET* [18] and our custom MLP-GAE, which uses a decoder based on concatenating the encoder outputs followed by a multilayer perceptron. Each model is tested under various experimental conditions to evaluate its performance within our proposed framework. The standard graph autoencoder (GAE) [7] is included to provide an undirected baseline model. Further details on model implementations and settings are provided in Appendix A.1.

### 4.3 Experimental Settings

For the three tasks described in Fig. 1, under the sampling defined in §3.3, we measure ROC-AUC (Receiver Operating Characteristic - Area Under the Curve) to evaluate a model’s ability to distinguish between classes, while AUPRC (Area Under Precision-Recall Curve) evaluates precision across different recall levels. We train the models according

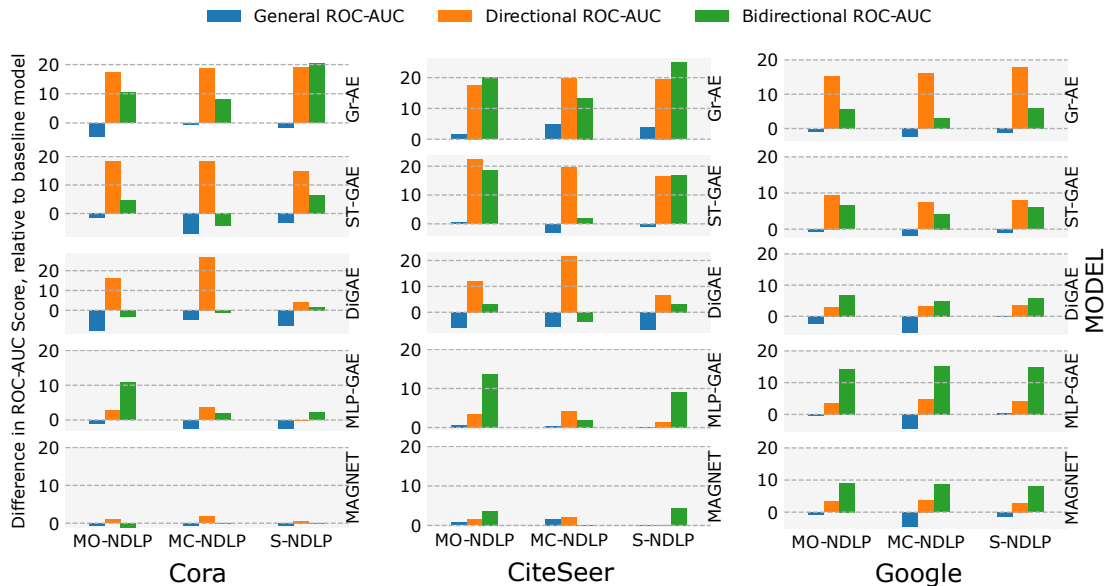


Figure 2: Performance difference of each proposed strategy compared to the baseline, measured in ROC-AUC (x100). Each bar represents the change in ROC-AUC - either an increase or decrease - when applying one of the proposed strategies to a specific sub-task, NDLP model, and dataset, relative to the same model’s baseline performance. Scores are averaged over 5 runs. Error bars are omitted for visual clarity.

to the strategies defined in §3, as well as a *Baseline* strategy. Namely, the model is trained on the *General DLP* training set with rebalancing of positive and negative edges’ contributions to training loss (Binary Cross Entropy). For each novel training strategy, we perform early stopping on the sum of ROC-AUC and AUPRC metrics over the *General DLP*, *Directional* and *Bidirectional* validation sets. Missing self-loops are always inserted for message passing, and they are also used as positive supervision samples in both *MO-NDLP* and *S-NDLP*, while they are treated as bidirectional negative supervision samples in *MC-NDLP*.

#### 4.4 Results

The performance results are summarized in Table 2 (Cora dataset), Table 3 (CiteSeer dataset), Table 4 (Google dataset) and in Figure 2. Performances are averaged over 5 random splits, keeping the same seed for all models. All ROC-AUC and AUPRC values are scaled by 100 for compactness and clearer visualization. In bold we highlight the best training strategy for each metric/model/task combination, while the underlined scores indicate the best training strategy across all models.

As a baseline, we evaluated an undirected graph autoencoder (GAE) model on the *General DLP* NDLP sub-task. While GAE performs deceptively well on the *General DLP* task, it fails to capture edge directionality, as expected. This is reflected in its random performance on the *Directional* task, with a ROC-AUC score of 0.5. This limitation arises from the inner product decoder used by GAE [7], which inherently assigns the same probability to both  $(u, v)$  and  $(v, u)$  edges. Results from this experiment are reported in the first rows of Tables 2, 3 and 4.

Our proposed strategies consistently improved performance on the *Directional* and on the *Bidirectional* tasks across all datasets and models, only slightly compromising (at times even benefiting) *General DLP* performance [18], with a few exceptions. For instance, *MAGNET* showed similar performance on Cora and CiteSeer, regardless of the training strategy, while it achieved significant improvement in the Bidirectional task on the Google dataset when trained using our strategies. This highlights that even though some models, like *MAGNET*, show limited gains on specific datasets, the overall benefits might be more pronounced in larger datasets like Google.

For other models like DiGAE, we observed a trade-off: its performance on the Directional task improved, but often at the expense of lower General task scores. Notably, on the Google dataset, especially with the S-NDLP strategy, DiGAE maintained its General task performance while delivering modest gains in Directional and Bidirectional tasks. Both MLP-GAE and MAGNET performed well on the Directional task but struggled on the General task, where

Table 2: ROC-AUC and AUPRC test scores of various models on Cora Dataset, trained with the *Baseline* and our proposed strategies.

		GENERAL		DIRECTIONAL		BIDIRECTIONAL	
		ROC-AUC	AUPRC	ROC-AUC	AUPRC	ROC-AUC	AUPRC
GAE	BASILINE	84.6 ± 0.4	88.6 ± 0.3	50.0 ± 0.0	50.0 ± 0.0	62.4 ± 3.0	64.0 ± 3.1
GR-GAE	BASILINE	<b>89.2 ± 0.4</b>	<b>92.4 ± 0.2</b>	63.4 ± 2.5	61.5 ± 2.7	69.1 ± 3.1	66.5 ± 3.3
	MO-NDLP	84.5 ± 1.1	86.3 ± 1.1	80.6 ± 0.7	80.2 ± 0.9	79.6 ± 4.3	84.6 ± 3.5
	MC-NDLP	88.6 ± 0.4	90.0 ± 0.4	82.1 ± 0.5	<b>81.8 ± 0.7</b>	77.3 ± 2.2	76.3 ± 1.7
	S-NDLP	87.8 ± 0.6	89.5 ± 0.5	<b>82.3 ± 0.5</b>	81.6 ± 0.4	<b>89.6 ± 1.6</b>	<b>92.4 ± 1.1</b>
ST-GAE	BASILINE	<b>87.8 ± 0.7</b>	<b>90.1 ± 0.5</b>	60.8 ± 0.5	64.5 ± 0.6	74.6 ± 1.8	74.1 ± 2.2
	MO-NDLP	86.3 ± 0.5	86.2 ± 0.4	<b>79.3 ± 1.0</b>	80.0 ± 0.9	79.3 ± 0.5	79.5 ± 1.9
	MC-NDLP	80.7 ± 2.0	80.1 ± 2.1	79.0 ± 2.3	<b>81.6 ± 1.9</b>	70.3 ± 3.0	68.1 ± 2.1
	S-NDLP	84.5 ± 0.4	84.9 ± 0.7	75.8 ± 1.0	78.4 ± 0.9	<b>81.1 ± 0.9</b>	<b>80.4 ± 1.6</b>
DiGAE	BASILINE	<b>80.4 ± 1.1</b>	<b>85.3 ± 0.8</b>	57.5 ± 1.3	63.0 ± 1.4	70.4 ± 2.2	68.6 ± 1.2
	MO-NDLP	70.2 ± 3.8	72.6 ± 3.6	73.6 ± 5.4	76.0 ± 4.2	67.3 ± 4.6	69.6 ± 4.1
	MC-NDLP	75.4 ± 0.9	77.4 ± 1.0	<b>84.3 ± 0.6</b>	<b>85.4 ± 0.8</b>	68.9 ± 1.5	69.3 ± 1.1
	S-NDLP	72.5 ± 4.0	77.4 ± 4.4	61.6 ± 1.3	69.2 ± 1.4	<b>72.1 ± 5.6</b>	<b>74.4 ± 5.7</b>
MLP-GAE	BASILINE	<b>77.1 ± 0.9</b>	<b>78.2 ± 0.6</b>	90.7 ± 0.6	90.7 ± 0.6	69.9 ± 3.2	69.7 ± 3.7
	MO-NDLP	76.0 ± 0.8	76.4 ± 0.7	93.4 ± 0.6	93.5 ± 0.6	<b>80.7 ± 1.6</b>	<b>79.2 ± 2.4</b>
	MC-NDLP	74.5 ± 0.7	75.6 ± 0.7	<b>94.3 ± 0.6</b>	<b>94.4 ± 0.5</b>	71.7 ± 2.4	65.7 ± 1.8
	S-NDLP	74.7 ± 1.0	74.9 ± 0.9	90.5 ± 0.7	90.0 ± 0.9	72.0 ± 2.6	70.5 ± 2.9
MAGNET	BASILINE	<b>75.2 ± 1.4</b>	<b>77.8 ± 1.0</b>	90.4 ± 0.9	89.8 ± 0.8	<b>71.9 ± 2.3</b>	<b>70.4 ± 2.8</b>
	MO-NDLP	74.4 ± 1.4	77.4 ± 1.1	91.3 ± 1.0	90.9 ± 1.0	70.6 ± 2.7	68.6 ± 2.7
	MC-NDLP	74.4 ± 1.0	77.4 ± 1.0	<b>92.1 ± 0.7</b>	<b>91.6 ± 0.7</b>	71.8 ± 2.6	70.0 ± 2.6
	S-NDLP	74.6 ± 1.3	77.5 ± 1.1	91.0 ± 1.0	90.4 ± 1.0	71.8 ± 2.8	70.2 ± 2.9

Table 3: ROC-AUC and AUPRC test scores of various models on CiteSeer Dataset, trained with the *Baseline* and our proposed strategies.

		GENERAL		DIRECTIONAL		BIDIRECTIONAL	
		ROC-AUC	AUPRC	ROC-AUC	AUPRC	ROC-AUC	AUPRC
GAE	BASILINE	78.6 ± 0.7	84.1 ± 0.6	50.0 ± 0.0	50.0 ± 0.0	56.2 ± 3.8	59.3 ± 1.9
GR-GAE	BASILINE	77.0 ± 0.7	84.3 ± 0.6	55.7 ± 2.3	58.2 ± 3.2	72.5 ± 3.7	71.3 ± 4.4
	MO-NDLP	78.6 ± 0.8	82.6 ± 1.3	73.4 ± 1.6	76.8 ± 1.2	92.6 ± 2.1	94.6 ± 1.5
	MC-NDLP	<b>81.9 ± 0.8</b>	<b>85.1 ± 0.5</b>	<b>75.5 ± 0.7</b>	<b>78.9 ± 0.6</b>	85.9 ± 2.8	85.1 ± 3.1
	S-NDLP	80.8 ± 0.9	84.4 ± 0.7	75.2 ± 1.0	78.2 ± 0.9	<b>97.5 ± 1.1</b>	<b>98.0 ± 0.7</b>
ST-GAE	BASILINE	80.9 ± 0.8	<b>85.2 ± 0.7</b>	56.0 ± 0.3	61.1 ± 0.5	72.0 ± 4.5	73.0 ± 3.7
	MO-NDLP	<b>81.4 ± 1.5</b>	82.6 ± 2.0	<b>78.5 ± 2.3</b>	<b>80.1 ± 1.8</b>	<b>90.5 ± 4.4</b>	<b>92.2 ± 4.1</b>
	MC-NDLP	77.8 ± 1.8	79.3 ± 2.4	75.5 ± 4.0	79.5 ± 2.8	73.9 ± 5.1	75.1 ± 4.9
	S-NDLP	80.0 ± 1.3	82.0 ± 1.4	72.6 ± 1.6	77.4 ± 1.1	88.9 ± 4.3	90.3 ± 3.9
DiGAE	BASILINE	<b>78.5 ± 0.9</b>	<b>83.5 ± 0.8</b>	56.6 ± 1.0	65.2 ± 1.5	62.3 ± 3.3	65.8 ± 3.8
	MO-NDLP	72.6 ± 5.0	74.9 ± 5.2	68.7 ± 3.4	71.7 ± 4.1	<b>65.6 ± 4.5</b>	70.8 ± 5.2
	MC-NDLP	72.7 ± 1.3	74.6 ± 0.9	<b>78.3 ± 2.9</b>	<b>80.1 ± 1.8</b>	58.6 ± 3.8	61.6 ± 3.3
	S-NDLP	71.8 ± 3.9	75.4 ± 4.6	63.3 ± 1.4	69.7 ± 2.2	65.5 ± 5.1	<b>71.5 ± 5.8</b>
MLP-GAE	BASILINE	73.3 ± 0.8	<b>76.1 ± 0.7</b>	88.4 ± 0.7	89.8 ± 0.6	76.5 ± 1.1	76.5 ± 2.6
	MO-NDLP	<b>74.0 ± 0.9</b>	75.2 ± 1.0	91.8 ± 0.5	92.2 ± 0.5	<b>90.2 ± 0.9</b>	<b>90.0 ± 1.4</b>
	MC-NDLP	73.7 ± 0.8	74.3 ± 0.9	<b>92.6 ± 0.5</b>	<b>92.9 ± 0.4</b>	78.5 ± 1.1	73.6 ± 2.4
	S-NDLP	73.3 ± 0.7	74.8 ± 0.9	89.8 ± 0.3	90.1 ± 0.3	85.5 ± 2.5	85.1 ± 2.4
MAGNET	BASILINE	71.6 ± 0.7	74.9 ± 0.8	89.5 ± 0.6	89.9 ± 0.6	70.9 ± 6.1	68.9 ± 6.6
	MO-NDLP	72.3 ± 0.6	74.7 ± 0.6	91.0 ± 0.6	91.2 ± 0.5	74.6 ± 7.1	73.4 ± 7.7
	MC-NDLP	<b>73.2 ± 0.9</b>	<b>75.2 ± 0.9</b>	<b>91.6 ± 0.6</b>	<b>91.7 ± 0.6</b>	71.1 ± 7.5	69.7 ± 7.5
	S-NDLP	71.3 ± 0.8	74.6 ± 0.8	89.6 ± 0.6	90.0 ± 0.5	<b>75.3 ± 6.2</b>	<b>73.5 ± 7.0</b>

their scores were systematically lower than those of the baseline GAE. DiGAE also struggled with the General task, surpassing GAE’s baseline performance only on the Google dataset.



Table 4: ROC-AUC and AUPRC test scores of various models on Google Dataset, trained with the *Baseline* and our proposed strategies.

		GENERAL		DIRECTIONAL		BIDIRECTIONAL	
		ROC-AUC	AUPRC	ROC-AUC	AUPRC	ROC-AUC	AUPRC
GAE	BASILINE	93.5 ± 0.2	94.9 ± 0.2	50.0 ± 0.0	50.0 ± 0.0	54.8 ± 0.8	53.6 ± 1.4
GR-GAE	BASILINE	<b>98.3 ± 0.1</b>	<b>98.9 ± 0.0</b>	76.5 ± 0.8	69.1 ± 0.9	92.0 ± 0.2	91.9 ± 0.2
	MO-NDLP	97.4 ± 0.1	98.1 ± 0.1	91.9 ± 0.2	90.3 ± 0.4	97.6 ± 0.1	97.6 ± 0.1
	MC-NDLP	95.7 ± 0.1	95.7 ± 0.1	92.6 ± 0.2	92.8 ± 0.1	95.1 ± 0.1	94.2 ± 0.1
	S-NDLP	96.9 ± 0.1	97.7 ± 0.0	<b>94.3 ± 0.1</b>	<b>94.7 ± 0.1</b>	<b>98.0 ± 0.0</b>	<b>98.5 ± 0.0</b>
ST-GAE	BASILINE	<b>98.4 ± 0.1</b>	<b>98.7 ± 0.0</b>	87.2 ± 0.2	86.2 ± 0.1	92.2 ± 0.3	89.6 ± 0.4
	MO-NDLP	97.6 ± 0.2	97.4 ± 0.3	<b>96.6 ± 0.1</b>	<b>96.8 ± 0.1</b>	<b>98.8 ± 0.1</b>	<b>98.6 ± 0.1</b>
	MC-NDLP	96.6 ± 0.1	96.4 ± 0.2	94.6 ± 0.1	96.1 ± 0.1	96.4 ± 0.1	95.9 ± 0.1
	S-NDLP	97.6 ± 0.0	97.5 ± 0.1	95.0 ± 0.1	96.0 ± 0.1	98.3 ± 0.1	96.8 ± 0.1
DiGAE	BASILINE	<b>97.0 ± 0.1</b>	<b>97.8 ± 0.1</b>	92.9 ± 0.2	94.5 ± 0.2	90.9 ± 0.3	87.7 ± 0.4
	MO-NDLP	94.7 ± 0.1	95.7 ± 0.2	95.9 ± 0.1	96.9 ± 0.1	<b>97.7 ± 0.1</b>	<b>97.9 ± 0.1</b>
	MC-NDLP	91.7 ± 0.6	92.4 ± 0.5	96.3 ± 0.2	<b>97.2 ± 0.1</b>	95.7 ± 0.3	95.5 ± 0.4
	S-NDLP	96.8 ± 0.1	97.3 ± 0.1	<b>96.5 ± 0.1</b>	97.0 ± 0.1	96.7 ± 0.2	96.3 ± 0.3
MLP-GAE	BASILINE	90.8 ± 0.1	91.6 ± 0.0	93.5 ± 0.1	94.4 ± 0.1	81.2 ± 0.2	77.8 ± 0.4
	MO-NDLP	90.4 ± 0.1	91.0 ± 0.1	97.0 ± 0.0	97.3 ± 0.0	95.6 ± 0.1	95.1 ± 0.1
	MC-NDLP	86.3 ± 0.1	87.9 ± 0.1	<b>98.4 ± 0.1</b>	<b>98.5 ± 0.1</b>	<b>96.4 ± 0.2</b>	95.4 ± 0.1
	S-NDLP	<b>91.2 ± 0.1</b>	<b>91.9 ± 0.1</b>	97.6 ± 0.0	97.8 ± 0.0	96.0 ± 0.1	<b>95.5 ± 0.1</b>
MAGNET	BASILINE	<b>89.1 ± 0.1</b>	<b>90.1 ± 0.0</b>	93.8 ± 0.6	94.3 ± 0.4	83.9 ± 2.0	77.7 ± 2.3
	MO-NDLP	88.5 ± 0.2	89.8 ± 0.1	97.1 ± 0.1	97.2 ± 0.1	<b>92.9 ± 0.1</b>	<b>91.1 ± 0.3</b>
	MC-NDLP	84.7 ± 0.7	86.2 ± 0.4	<b>97.6 ± 0.0</b>	<b>97.3 ± 0.1</b>	92.5 ± 0.2	88.9 ± 0.3
	S-NDLP	87.9 ± 0.3	89.4 ± 0.2	96.7 ± 0.1	96.8 ± 0.1	91.9 ± 0.5	88.3 ± 0.9

Selecting the right model-strategy combination depends on how much one is willing to sacrifice General task performance for improvements in Directional and Bidirectional tasks. Interestingly, this trade-off is not always necessary. For example, with the CiteSeer dataset, Gravity-GAE with MC-NDLP achieved the best General task performance while significantly improving Directional and Bidirectional scores. However, the optimal combination of model and strategy varies by dataset. For the Cora dataset, Gravity-AE with S-NDLP offers a balanced solution, delivering strong Directional and Bidirectional performance with only a slight reduction in General task scores. On the CiteSeer dataset, ST-GAE with MO-NDLP provides a good balance, offering competitive General task performance alongside noticeable gains in Directional and Bidirectional tasks. Similarly, for the Google dataset, ST-GAE with MO-NDLP proves to be an excellent choice, delivering significant improvements in Directional and Bidirectional tasks with minimal sacrifice in General task performance.

## 5 Conclusions

In this paper, we introduced and evaluated new training strategies to improve performance on Neural Directed Link Prediction tasks, addressing the limitations of current models in learning edge directionality. By extending existing models to handle multiple sub-tasks simultaneously, we demonstrated that the proposed strategies – Multi-Class (MC-DLP), Scalarization-based (S-DLP), and Multi-Objective (MO-DLP) Directed Link Prediction – consistently improve performance on both Directional and Bidirectional tasks, although at times with a trade-off in General task performance.

While no single approach universally outperforms across all settings, the flexibility offered by our proposed training strategies provides a powerful means for improving NDLP model capabilities. Future work can focus on refining these strategies to minimize trade-offs, particularly for applications that demand robust handling of directed graphs and directed link prediction. Our training strategies for learning edge directionality might also be usefully combined with approaches that allow GNNs to better represent edge directionality. Many alternative encodings [4,5] and labeling tricks [1,2,3] have been proposed to enhance the expressiveness of GNNs, also for performing DLP, and it would be interesting to explore a wider range of augmented models. Simultaneous training across the three facets of DLP allows for more concise comparative studies to be done on the ability of models, and various enhancements, to provide balanced performance across the three facets of DLP. Also, an interesting area for future exploration is knowledge graphs (KG), which could greatly benefit from our methods. Since KG-oriented tasks often employ specialized losses

with margin terms [46] and involve complex query answering rather than basic link prediction [47], studying how enhanced directionality learning impacts KG performance would be a valuable direction.

## References

- [1] Réka Albert and Albert-László Barabási. Statistical mechanics of complex networks. *Reviews of modern physics*, 74(1):47, 2002.
- [2] Weihua Hu, Matthias Fey, Marinka Zitnik, Yuxiao Dong, Hongyu Ren, Bowen Liu, Michele Catasta, and Jure Leskovec. Open graph benchmark: datasets for machine learning on graphs. In *Proceedings of the 34th International Conference on Neural Information Processing Systems, NIPS’20*, Red Hook, NY, USA, 2020. Curran Associates Inc. ISBN 9781713829546.
- [3] Aidan Hogan, Eva Blomqvist, Michael Cochez, Claudia d’Amato, Gerard De Melo, Claudio Gutierrez, Sabrina Kirrane, José Emilio Labra Gayo, Roberto Navigli, Sebastian Neumaier, et al. Knowledge graphs. *ACM Computing Surveys (Csur)*, 54(4):1–37, 2021.
- [4] Petter Holme and Jari Saramäki. *Temporal Network Theory*. Springer International Publishing, 2019. ISBN 9783030234959.
- [5] Xin Li and Hsinchun Chen. Recommendation as link prediction: a graph kernel-based machine learning approach. In *Proceedings of the 9th ACM/IEEE-CS Joint Conference on Digital Libraries, JCDL ’09*, page 213–216, New York, NY, USA, 2009. Association for Computing Machinery. ISBN 9781605583228.
- [6] Linyuan Lü and Tao Zhou. Link prediction in complex networks: A survey. *Physica A: Statistical Mechanics and its Applications*, 390(6):1150–1170, 2011.
- [7] Thomas N Kipf and Max Welling. Variational graph auto-encoders. *arXiv preprint arXiv:1611.07308*, 2016.
- [8] Jie Wang, Jiye Liang, Kaixuan Yao, Jianqing Liang, and Dianhui Wang. Graph convolutional autoencoders with co-learning of graph structure and node attributes. *Pattern Recognition*, 121:108215, 2022.
- [9] Muhan Zhang and Yixin Chen. Link prediction based on graph neural networks. In *Proceedings of the 32nd International Conference on Neural Information Processing Systems*, page 5171–5181, 2018.
- [10] Lei Cai and Shuiwang Ji. A multi-scale approach for graph link prediction. *Proceedings of the AAAI Conference on Artificial Intelligence*, 34(04):3308–3315, Apr. 2020.
- [11] Xinyu Fu, Jiani Zhang, Ziqiao Meng, and Irwin King. Magnn: Metapath aggregated graph neural network for heterogeneous graph embedding. *WWW ’20*, page 2331–2341, New York, NY, USA, 2020. Association for Computing Machinery. ISBN 9781450370233.
- [12] Chaobo He, Junwei Cheng, Xiang Fei, Yu Weng, Yulong Zheng, and Yong Tang. Community preserving adaptive graph convolutional networks for link prediction in attributed networks. *Knowledge-Based Systems*, 272:110589, 2023.
- [13] G. Kollias, Vasileios Kalantzis, Tsuyoshi Id’e, Aurélie C. Lozano, and Naoki Abe. Directed graph auto-encoders. In *AAAI Conference on Artificial Intelligence*, 2022.
- [14] Yusen Zhang, Yusong Tan, Songlei Jian, Qingbo Wu, and Kenli Li. DGLP: Incorporating orientation information for enhanced link prediction in directed graphs. In *ICASSP 2024-2024 IEEE International Conference on Acoustics, Speech and Signal Processing (ICASSP)*, pages 6565–6569. IEEE, 2024.
- [15] Changxiang He, Jiayuan Zeng, Yan Li, Shuting Liu, Lele Liu, and Chen Xiao. Two-stream signed directed graph convolutional network for link prediction. *Physica A: Statistical Mechanics and its Applications*, 605:128036, 2022.
- [16] Tao Yi, Shanfan Zhang, Zhan Bu, Jinwei Du, and Changjian Fang. Link prediction based on higher-order structure extraction and autoencoder learning in directed networks. *Knowledge-Based Systems*, 241:108241, 2022.
- [17] Guillaume Salha, Stratis Limnios, Romain Hennequin, Viet-Anh Tran, and Michalis Vazirgiannis. Gravity-inspired graph autoencoders for directed link prediction. In *Proceedings of the 28th ACM International Conference on Information and Knowledge Management*, page 589–598, 2019.
- [18] Xitong Zhang, Yixuan He, Nathan Brugnone, Michael Perlmutter, and Matthew Hirn. Magnet: A neural network for directed graphs. In *Advances in Neural Information Processing Systems*, 2021.
- [19] Shanfan Zhang, Wenjiao Zhang, Zhan Bu, and Xia Zhang. Clusterlp: A novel cluster-aware link prediction model in undirected and directed graphs. *International Journal of Approximate Reasoning*, 172:109216, 2024.

- [20] Antoine Bordes, Nicolas Usunier, Alberto Garcia-Duran, Jason Weston, and Oksana Yakhnenko. Translating embeddings for modeling multi-relational data. In *Advances in Neural Information Processing Systems*, volume 26, 2013.
- [21] Martin Simonovsky and Nikos Komodakis. Graphvae: Towards generation of small graphs using variational autoencoders. In Věra Kůrková, Yannis Manolopoulos, Barbara Hammer, Lazaros Iliadis, and Ilias Maglogiannis, editors, *Artificial Neural Networks and Machine Learning – ICANN 2018*, pages 412–422, Cham, 2018. Springer International Publishing.
- [22] Dan Lin, Jiajing Wu, Qi Xuan, and Chi K. Tse. Ethereum transaction tracking: Inferring evolution of transaction networks via link prediction. *Physica A: Statistical Mechanics and its Applications*, 600:127504, 2022.
- [23] Ajay Kumar, Shashank Sheshar Singh, Kuldeep Singh, and Bhaskar Biswas. Link prediction techniques, applications, and performance: A survey. *Physica A: Statistical Mechanics and its Applications*, 553:124289, 2020.
- [24] Meng Qin and Dit-Yan Yeung. Temporal link prediction: A unified framework, taxonomy, and review. *ACM Comput. Surv.*, 56(4), nov 2023.
- [25] Haixia Wu, Chunyao Song, Yao Ge, and Tingjian Ge. Link prediction on complex networks: An experimental survey. *Data Science and Engineering*, 7(3):253–278, June 2022.
- [26] Djihad Arrar, Nadjet Kamel, and Abdelaziz Lakhfif. A comprehensive survey of link prediction methods. *The Journal of Supercomputing*, September 2023.
- [27] Emanuele Rossi, Bertrand Charpentier, Francesco Di Giovanni, Fabrizio Frasca, Stephan Günnemann, and Michael M. Bronstein. Edge Directionality Improves Learning on Heterophilic Graphs. In *Proceedings of the Second Learning on Graphs Conference*, pages 25:1–25:27. PMLR, April 2024. ISSN: 2640-3498.
- [28] Shijie Zhu, Jianxin Li, Hao Peng, Senzhang Wang, and Lifang He. Adversarial directed graph embedding. *Proceedings of the AAAI Conference on Artificial Intelligence*, 35(5):4741–4748, May 2021.
- [29] Jean-Antoine Désidéri. Multiple-gradient descent algorithm (mgda) for multiobjective optimization. *Comptes Rendus Mathématique*, 350(5):313–318, 2012.
- [30] Yuzheng Hu, Ruicheng Xian, Qilong Wu, Qiuling Fan, Lang Yin, and Han Zhao. Revisiting scalarization in multi-task learning: A theoretical perspective. *Advances in Neural Information Processing Systems*, 36, 2024.
- [31] Justin Gilmer, Samuel S. Schoenholz, Patrick F. Riley, Oriol Vinyals, and George E. Dahl. Neural message passing for quantum chemistry. In *Proceedings of the 34th International Conference on Machine Learning - Volume 70*, ICML’17, page 1263–1272. JMLR.org, 2017.
- [32] William L. Hamilton, Rex Ying, and Jure Leskovec. Inductive representation learning on large graphs. In *Proceedings of the 31st International Conference on Neural Information Processing Systems*, page 1025–1035, 2017.
- [33] Petar Veličković, Guillem Cucurull, Arantxa Casanova, Adriana Romero, Pietro Liò, and Yoshua Bengio. Graph attention networks. In *International Conference on Learning Representations*, 2018.
- [34] Keyulu Xu, Weihua Hu, Jure Leskovec, and Stefanie Jegelka. How powerful are graph neural networks? In *International Conference on Learning Representations*, 2019.
- [35] Michaël Defferrard, Xavier Bresson, and Pierre Vandergheynst. Convolutional neural networks on graphs with fast localized spectral filtering. In *Proceedings of the 30th International Conference on Neural Information Processing Systems*, NIPS’16, page 3844–3852, Red Hook, NY, USA, 2016. Curran Associates Inc. ISBN 9781510838819.
- [36] Thomas N Kipf and Max Welling. Semi-supervised classification with graph convolutional networks. *arXiv preprint arXiv:1609.02907*, 2016.
- [37] Patrick Reiser, Marlen Neubert, André Eberhard, Luca Torresi, Chen Zhou, Chen Shao, Houssam Metni, Clint van Hoesel, Henrik Schopmans, Timo Sommer, and Pascal Friederich. Graph neural networks for materials science and chemistry. *Communications Materials*, 3(1), November 2022.
- [38] Ming Jin, Huan Yee Koh, Qingsong Wen, Daniele Zambon, Cesare Alippi, Geoffrey I Webb, Irwin King, and Shirui Pan. A survey on graph neural networks for time series: Forecasting, classification, imputation, and anomaly detection. *IEEE Transactions on Pattern Analysis and Machine Intelligence*, 2024.
- [39] Fredrik Johannessen and Martin Jullum. Finding money launderers using heterogeneous graph neural networks. *arXiv preprint arXiv:2307.13499*, 2023.
- [40] Mark Weber, Giacomo Domeniconi, Jie Chen, Daniel Karl I Weidele, Claudio Bellei, Tom Robinson, and Charles E Leiserson. Anti-money laundering in bitcoin: Experimenting with graph convolutional networks for financial forensics. *arXiv preprint arXiv:1908.02591*, 2019.

- [41] Béni Egressy, Luc Von Niederhäusern, Jovan Blanuša, Erik Altman, Roger Wattenhofer, and Kubilay Atasü. Provably powerful graph neural networks for directed multigraphs. In *Proceedings of the AAAI Conference on Artificial Intelligence*, volume 38, pages 11838–11846, 2024.
- [42] Erik Altman, Jovan Blanuša, Luc Von Niederhäusern, Béni Egressy, Andreea Anghel, and Kubilay Atasü. Realistic synthetic financial transactions for anti-money laundering models. *Advances in Neural Information Processing Systems*, 36, 2024.
- [43] Nino Shervashidze, Pascal Schweitzer, Erik Jan van Leeuwen, Kurt Mehlhorn, and Karsten M. Borgwardt. Weisfeiler-lehman graph kernels. *Journal of Machine Learning Research*, 12(77):2539–2561, 2011.
- [44] Jintang Li, Ruofan Wu, Wangbin Sun, Liang Chen, Sheng Tian, Liang Zhu, Changhua Meng, Zibin Zheng, and Weiqiang Wang. What’s behind the mask: Understanding masked graph modeling for graph autoencoders. In *Proceedings of the 29th ACM SIGKDD Conference on Knowledge Discovery and Data Mining*, page 1268–1279, 2023.
- [45] Eric A Hagberg, Daniel A Schult, and Pieter J Swart. Exploring Network Structure, Dynamics, and Function using NetworkX. In *Proceedings of the 7th Python in Science Conference*, page 5, Pasadena, CA, 2008.
- [46] Antoine Bordes, Nicolas Usunier, Alberto Garcia-Duran, Jason Weston, and Oksana Yakhnenko. Translating embeddings for modeling multi-relational data. *Advances in neural information processing systems*, 26, 2013.
- [47] Hongyu Ren, Weihua Hu, and Jure Leskovec. Query2box: Reasoning over knowledge graphs in vector space using box embeddings. *arXiv preprint arXiv:2002.05969*, 2020.
- [48] Yixuan He, Xitong Zhang, Junjie Huang, Benedek Rozemberczki, Mihai Cucuringu, and Gesine Reinert. Pytorch geometric signed directed: A software package on graph neural networks for signed and directed graphs. In *Learning on Graphs Conference*, pages 12–1. PMLR, 2024.
- [49] Diederik P Kingma and Jimmy Ba. Adam: A method for stochastic optimization. *arXiv preprint arXiv:1412.6980*, 2014.

## A Appendix

### A.1 Models

We test our three frameworks on different NDLP models found throughout the literature. All the models we tried fall within the Graph Autoencoder paradigm. In the following, assuming  $\vec{z}_v \in \mathbb{R}^L$  is the output encoder embedding for node  $v$ ,  $\hat{p}_{uv}$  is the predicted probability of edge  $e_{uv}$  and  $\sigma$  is the sigmoid function. We present a brief description for each of them.

Assuming  $\vec{z}_v \in \mathbb{R}^L$  is the output encoder embedding for node  $v$ ,  $\hat{p}_{uv}$  is the predicted probability of edge  $e_{uv}$  and  $\sigma$  is the sigmoid function.

#### A.1.1 GAE

The encoder has 2 layers, with input dimension equal to the number of nodes of the graph it is trained on (due to OHE), hidden dimension 64 and output dimension 32. For more details, see [7].

#### A.1.2 Gravity-GAE

The encoder is given by two layers of:

$$H^{l+1} = D_{\text{out}}^{-1} \tilde{A} X W$$

Where  $\tilde{A} = A + I$  and  $D_{\text{out}}^{-1}$  is the out-degree diagonal matrix of  $\tilde{A}$ . The input dimension is equal to the number of nodes (due to OHE), hidden dimension is 64 and output dimension 32.

Its decoder is given by:

$$\hat{p}_{uv} = \sigma(\vec{z}_v[0] - \lambda \ln(\|\vec{z}_u[1:] - \vec{z}_v[1:] \|_2^2))$$

Taken from [17].

#### A.1.3 Source/Target GAE

Assuming  $L$  is even, Its decoder is given by:

$$\hat{p}_{uv} = \sigma(\vec{z}_v[:\frac{L}{2}] \cdot \vec{z}_u[\frac{L}{2}:])$$

Taken from [17]. Encoder and dimensions as Gravity-GAE.

#### A.1.4 MLP-GAE

In all frameworks except *MC-NDLP*, its decoder is given by:

$$\hat{p}_{uv} = MLP(\vec{z}_v || \vec{z}_u)$$

Where  $||$  represents concatenation. In the *MC-NDLP* framework, it's defined as in 3.1. In both cases, the MLP has only one layer which allows for a much faster implementation (although specific to DLP). Encoder and dimensions as Gravity-GAE.

#### A.1.5 DIGAE

The encoder is given by:

$$\begin{cases} \vec{z}_v^S &= \tilde{A} \sigma(\tilde{A}^T \vec{x}_v W_S^{(0)}) W_S^{(1)} \\ \vec{z}_v^T &= \tilde{A}^T \sigma(\tilde{A} \vec{x}_v W_T^{(0)}) W_T^{(1)} \end{cases} \quad (7)$$

And the decoder is the same as *Source/Target-GAE*, where we recognize:

$$\begin{cases} \bar{z}_v^S &= \bar{z}_v[: \frac{L}{2}] \\ \bar{z}_v^T &= \bar{z}_v[\frac{L}{2} :] \end{cases} \quad (8)$$

For further details, see [13].

### A.1.6 MAGNET

The *MAGNET* model is described in [18]. It consists of a GCN where the aggregation is performed via the Magnetic Laplacian, i.e. a complex hermitian matrix that transfers to directed graphs several useful properties once exclusively held by laplacians of undirected networks such as positive definitions.

## A.2 Hyperparameters

All models have two encoder layers. All have the following hyperparameters:

- *input dimension*: always equal to the number of nodes in the graph, except for MAGNET where it is 2 (in- and out-degree);
- *hidden dimension*: equal to 64 for all models across datasets except MAGNET which has 16;
- *output dimension*: set to 32 for all models across datasets except MAGNET that is configured as in [18] with few modifications (see below);
- *number of epochs*: set to 1000 for all models across datasets except MAGNET which has 3000.

The  $\lambda$  parameter of Gravity-GAE is initially set across datasets as in [17], but it is subsequently trained together with all other model parameters. Notably, we started it from  $\lambda = 0.1$  when training for Multi-Class on Google for convergence reasons.

The  $\alpha$  and  $\beta$  parameters of DiGAE have been set to 0.5 and not trained due to occasional instability.

MLP-GAE and MAGNET have a custom one-layer MLP decoder specifically designed to compute the probability of each edge given its vertices' embeddings in an efficient way. It represents the same functions as a standard MLP, but its internal matrix operations have been reordered specifically for DLP. It has 0.5 dropout.

MAGNET's  $q$  parameter has been set to 0.05 and not trained to isolate our frameworks' effects, being it directly linked to directionality embedding [18].

MAGNET's implementation has been taken from Pytorch Geometric Signed Directed [48] and slightly modified to accomodate the custom MLP decoder. The order of the Chebyshev polynomial is 2 everywhere.

All models make use of early stopping. The validation metric is the sum of ROC-AUC and AP-AUC on the *General* validation set and on the *General, Directional and Bidirectional* validation sets respectively for the Baseline and all the other training frameworks. patience is set to 200 for all models except for MagNet under the Multi-Class framework where it was set to 30 to keep computational time tractable.

All missing self-loops were always added as positive training targets for the Baseline, Multi-Objective and Scalarization frameworks, while they were treated as negatives in the Multi-Class framework according to empirical trials and for standardization.

Adam optimizer was used to train all models [49], that were implemented in PyTorch. Learning rates are summarized in 5 except for GAE that has  $lr = 0.05$  for all Baseline trainings. Weight decay has been set to  $5e-4$  for MAGNET only.

All models' hyperparameters values have either been taken from the respective papers or empirically tuned to achieve stable learning across novel techniques.

### A.3 Statistical Independence in the Multi-Class approach

In order to prove Equation 4, it suffices to prove that probabilities properly factorize:

$$\hat{p}_{uv}^{pb} = \hat{P}(e_{uv}, e_{vu} | A, X) = \hat{P}(e_{uv} | e_{vu}, A, X) \hat{P}(e_{vu} | A, X) = \hat{P}(e_{uv} | A, X) \hat{P}(e_{vu} | A, X) \quad (9)$$

And similarly for the other cases. We therefore proved that joint probabilities can be factorized and therefore Equation 4 applies.

Table 5: Models’ learning rates

Dataset	Method	Model	lr
Cora	Baseline, Multi-Objective & Scalarization	GR-AE	0.01
		ST-GAE	0.01
		MLP-GAE	0.002
		DiGAE	0.02
		MAGNET	0.001
	Multi-Class	GR-AE	0.01
		ST-GAE	0.01
		MLP-GAE	0.001
		DiGAE	0.02
		MAGNET	0.001
Citeseer	Baseline, Multi-Objective & Scalarization	GR-AE	0.05
		ST-GAE	0.02
		MLP-GAE	0.002
		DiGAE	0.02
		MAGNET	0.001
	Multi-Class	GR-AE	0.01
		ST-GAE	0.01
		MLP-GAE	0.001
		DiGAE	0.02
		MAGNET	0.001
Citeseer	Baseline, Multi-Objective & Scalarization	GR-AE	0.05
		ST-GAE	0.01
		MLP-GAE	0.002
		DiGAE	0.02
		MAGNET	0.001
	Multi-Class	GR-AE	0.01
		ST-GAE	0.01
		MLP-GAE	0.002
		DiGAE	0.002
		MAGNET	0.001